Diluted magnetic semiconductors with narrow band gaps

Bo Gu [1*] and Sadamichi Maekawa[1,2]

[1] *Advanced Science Research Center,*

Japan Atomic Energy Agency, Tokai 319-1195, Japan

[2] *ERATO, Japan Science and Technology Agency, Sendai 980-8577, Japan*

(Dated: November 16, 2016)

Abstract

We propose a method to realize diluted magnetic semiconductors (DMSs) with p- and n-type carriers by choosing host semiconductors with a narrow band gap. By employing a combination of the density function theory and quantum Monte Carlo simulation, we demonstrate such semiconductors using Mn-doped $BaZn_2As_2$, which has a band gap of 0.2 eV. In addition, we found a nontoxic DMS Mn-doped $BaZn_2Sb_2$, of which the Curie temperature T_c is predicted to be higher than that of Mn-doped $BaZn_2As_2$, the T_c of which was up to 230 K in a recent experiment.

PACS numbers: 75.50.Pp, 75.30.Hx, 02.70.Ss

I. INTRODUCTION

After the discovery of ferromagnetism in (Ga,Mn)As, diluted magnetic semiconductors (DMSs) have received considerable attention owing to potential applications based on the use of both their charge and spin degrees of freedom in electronic devices[1,2]. Thus far, the highest Curie temperature of (Ga,Mn)As has been $T_c = 190$ K[3]. The substitution of divalent Mn atoms into trivalent Ga sites introduces hole carriers; thus, (Ga,Mn)As is a p-type DMS. The valence mismatch between Mn and Ga leads to severely limited chemical solubility for Mn in GaAs. Moreover, owing to simultaneous doping of charge and spin induced by Mn substitution, it is difficult to individually optimize charge and spin densities.

To overcome these difficulties, a new type of DMS, i.e., Li(Zn,Mn)As was proposed[4] and later fabricated with $T_c = 50$ K[5]. It is based on LiZnAs, a I−II−V semiconductor. Spin is introduced by isovalent (Zn^{2+}, Mn^{2+}) substitution, which is decoupled from carrier doping with excess/deficient Li concentration. Although Li(Zn,Mn)As was proposed as a promising n-type DMS with excess Li^+, p-type carriers were obtained in the experiment with excess Li. The introduction of holes was presumably because of the excess Li^+ in substitutional Zn^{2+} sites[5]. Later, another I−II−V DMS, i.e., Li(Zn,Mn)P was reported in an experiment with $T_c = 34$ K[6]. Li(Zn,Mn)P with excess Li was determined to be of the p-type as well in the experiment. According to first-principles calculations, the reason for this is the same as that for Li(Zn,Mn)As[6]. Although such p-type I−II−V DMSs have a few distinct advantages over (Ga,Mn)As, the achievable T_c is much lower than that of (Ga,Mn)As.

Another type of DMS (Ba,K)(Zn,Mn)$_2$As$_2$ was observed in experiments with T_c up to 230 K[7,8], which is higher than that for (Ga,Mn)As. Based on the semiconductor BaZn$_2$As$_2$, holes were doped by (Ba^{2+}, K^+) substitutions, and spins by isovalent (Zn^{2+}, Mn^{2+}) substitutions. It was a p-type DMS. Motivated by the high T_c, density functional theory (DFT) calculations[9] and photoemission spectroscopy experiments[10,11] were conducted to understand the microscopic mechanism of ferromagnetism of p-type DMS (Ba,K)(Zn,Mn)$_2$As$_2$. By contrast, an n-type DMS, i.e., Ba(Zn,Mn,Co)$_2$As$_2$ was recently reported in an experiment with $T_c \sim 80$ K[12]. In this material, electrons are doped because of the substitution of Zn with Co, and spins are generated mainly because of (Zn^{2+}, Mn^{2+}) substitutions.

In Mn-doped BaZn$_2$As$_2$, why is the ferromagnetic (FM) coupling observed in both p- and n-type cases? Why is T_c much lower in the n-type case than that in the p-type case? In
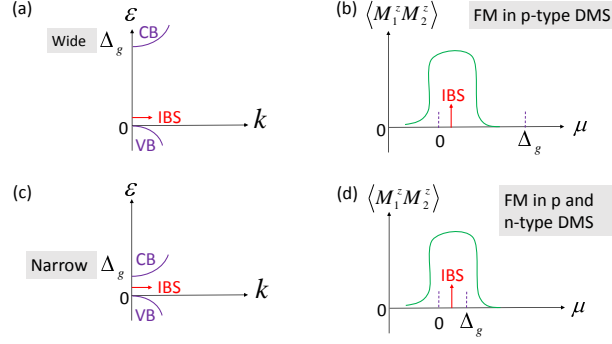
FIG. 1. Schematic pictures of an impurity bound state (IBS) and ferromagnetic (FM) coupling in diluted magnetic semiconductors (DMSs). (a) Host bands $\epsilon(k)$ with a wide band gap Δ_g between the valence band (VB) and the conduction band (CB). The position of the IBS ω_{IBS} (arrow) is close to the top of the VB owing to strong mixing between the impurity and the VB, and usually no IBS appears below the bottom of the CB because of weak mixing between the impurity and the CB[13–15]. We have $0 \lesssim \omega_{IBS} \ll \Delta_g$. (b) Magnetic correlation $\langle M_1^z M_2^z \rangle$ between two impurities as a function of the chemical potential μ for case (a). Positive $\langle M_1^z M_2^z \rangle$ denotes FM coupling, which can be developed when $\mu \sim \omega_{IBS}$[16–18]. Hence, for p-type carriers ($\mu \sim 0$), FM coupling can be obtained as $\mu \sim \omega_{IBS}$, and for n-type carriers ($\mu \sim \Delta_g$), no magnetic coupling is obtained between impurities because $\mu \gg \omega_{IBS}$[13–15]. (c) Similar to case (a), except for a narrow Δ_g. By choosing suitable host semiconductors and impurities, the condition $0 \lesssim \omega_{IBS} \lesssim \Delta_g$ is obtained. (d) Similar to case (b), except for a narrow Δ_g. FM coupling can be achieved for both p-type and n-type carriers when $\mu \sim \omega_{IBS}$. In this study, we describe cases (c) and (d).

general, can p- and n-type DMSs be realized? The answers will be helpful for fabricating spin p-n junctions in the future. In this study, we attempt to address such issues. In previous studies on DMS materials with wide band gap Δ_g, we found that the position of the impurity bound state (IBS) ω_{IBS} was close to the top of the valence band (VB) owing to the strong mixing between the impurity and the VB, and usually no IBS appeared below the bottom of the conduction band (CB) because of weak mixing between the impurity and the CB[13–15]. Thus, we have $0 \lesssim \omega_{IBS} \ll \Delta_g$, as shown in Fig. 1(a). The magnetic correlation $\langle M_1^z M_2^z \rangle$ between two impurities with FM coupling (positive $\langle M_1^z M_2^z \rangle$) can be determined when the chemical potential μ is tuned to be close to the IBS: $\mu \sim \omega_{IBS}$[16–18]. Therefore, for p-type carriers ($\mu \sim 0$), FM coupling can be obtained as $\mu \sim \omega_{IBS}$, and for n-type carriers ($\mu \sim$

3

Δ_g), no magnetic coupling is obtained between impurities because $\mu \gg \omega_{IBS}$. A schematic diagram describing p-type DMS materials with a wide band gap, including (Zn,Mn)O[13], (Ga,Mn)As[14], and Mg(O,N)[15], is shown in Fig. 1 (b).

Here, we propose a method for realizing p- and n-type DMS. The key is choosing host semiconductors with a narrow band gap Δ_g. By selecting suitable host semiconductors and impurities, the condition $0 \lesssim \omega_{IBS} \lesssim \Delta_g$ is satisfied, as shown in Fig. 1(c). We show that for both the p-type ($\mu \sim 0$) and the n-type ($\mu \sim \Delta_g$) cases, the condition for developing FM coupling, that is $\mu \sim \omega_{IBS}$, can be fulfilled, as shown in Fig. 1(d).

II. DFT+QMC METHOD

In the following, we realistically calculate the electronic and magnetic properties of the Mn-doped BaZn$_2$As$_2$ DMS, which has a narrow band gap Δ_g (= 0.2 eV)[7]. We use a combination of the DFT[19,20] and the Hirsch−Fye quantum Monte Carlo (QMC) simulation[21]. Our combined DFT+QMC method can be used for an in-depth treatment of the band structures of materials and strong electron correlations of magnetic impurities on an equal footing; thus, it can be applied for designing functional semiconductor-[13–15] and metal-based[22–24] materials. The method involves two calculations steps. First, the Haldane−Anderson impurity model[25] is formulated within the local density approximation for determining the host band structure and impurity-host mixing. Second, magnetic correlations of the Haldane-Anderson impurity model at finite temperatures are calculated using the Hirsch−Fye QMC technique[21].

The Haldane−Anderson impurity model is defined as follows:

$$H = \sum_{\mathbf{k},\alpha,\sigma}[\epsilon_\alpha(\mathbf{k}) - \mu]c^\dagger_{\mathbf{k}\alpha\sigma}c_{\mathbf{k}\alpha\sigma} + \sum_{\mathbf{k},\alpha,\mathbf{i},\xi,\sigma}(V_{\mathbf{i}\xi\mathbf{k}\alpha}d^\dagger_{\mathbf{i}\xi\sigma}c_{\mathbf{k}\alpha\sigma}$$
$$+ h.c.) + (\epsilon_d - \mu)\sum_{\mathbf{i},\xi,\sigma}d^\dagger_{\mathbf{i}\xi\sigma}d_{\mathbf{i}\xi\sigma} + U\sum_{\mathbf{i},\xi}n_{\mathbf{i}\xi\uparrow}n_{\mathbf{i}\xi\downarrow}, \qquad (1)$$

where $c^\dagger_{\mathbf{k}\alpha\sigma}$ ($c_{\mathbf{k}\alpha\sigma}$) is the creation (annihilation) operator for a host electron with wave vector $\mathbf{k}$ and spin σ in the VB ($\alpha = v$) or the CB ($\alpha = c$), and $d^\dagger_{\mathbf{i}\xi\sigma}$ ($d_{\mathbf{i}\xi\sigma}$) is the creation (annihilation) operator for a localized electron at impurity site $\mathbf{i}$ in orbital ξ and spin σ with $n_{\mathbf{i}\xi\sigma} = d^\dagger_{\mathbf{i}\xi\sigma}d_{\mathbf{i}\xi\sigma}$. Here, $\epsilon_\alpha(\mathbf{k})$ is the host band dispersion, μ is the chemical potential, $V_{\mathbf{i}\xi\mathbf{k}\alpha}$ denotes mixing between the impurity and the host, ϵ_d is the impurity $3d$ orbital energy,
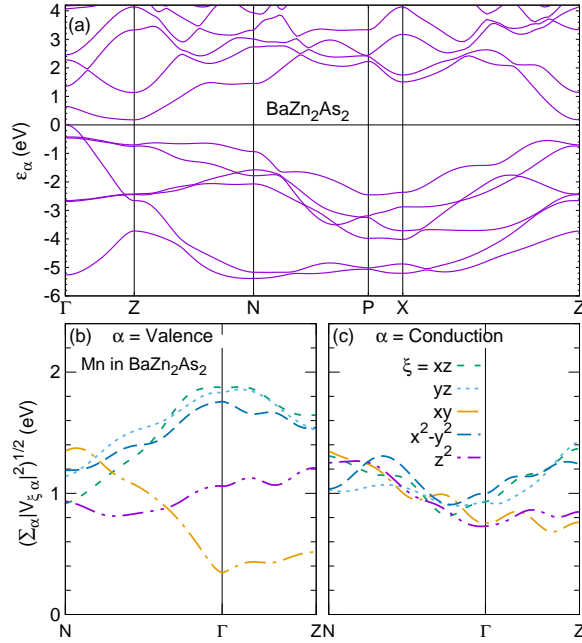
FIG. 2. Host band and mixing parameters of Mn-doped $BaZn_2As_2$. (a) Energy bands ϵ_α of host $BaZn_2As_2$, which has space group I4/mmm. An indirect band gap of 0.2 eV was obtained by DFT calculations, which agrees well with the experimental value[7]. The mixing function between the ξ orbitals of an Mn impurity and $BaZn_2As_2$ hosts (b) valence bands and (c) conduction bands.

and U is the on-site Coulomb repulsion of the impurity. Considering the condition of Hund coupling $J_H \ll U$, J_H is neglected and the single-orbital approximation is used to describe the magnetic sates of impurities.

III. RESULTS FOR $Ba(Zn, Mn)_2As_2$

The parameters $\epsilon_\alpha(\mathbf{k})$ and $V_{\mathbf{i}\xi\mathbf{k}\alpha}$ are obtained by DFT calculations using the Wien2k package[26]. To reproduce the experimental narrow band gap of 0.2 eV in $BaZn_2As_2$[7], we use the modified Becke−Johnsom exchange potential (mBJ)[27], which has been implemented in the Wien2k package. The obtained energy band $\epsilon_\alpha(\mathbf{k})$ is shown in Fig. 2 (a), where $BaZn_2As_2$ has space group I4/mmm. We obtained an indirect gap band $\Delta_g = 0.2$ eV, which is in good agreement with the experimental[7] and previous calculated[10,28] values.

The mixing parameter between the ξ orbitals of an Mn impurity and the $BaZn_2As_2$ host

is defined as $V_{\mathbf{i}\xi\mathbf{k}\alpha}\equiv\langle\varphi_\xi(\mathbf{i})|H|\Psi_\alpha(\mathbf{k})\rangle\equiv\frac{1}{\sqrt{N}}e^{i\mathbf{k}\cdot\mathbf{i}}V_{\xi\alpha}(\mathbf{k})$, which can be expressed as

$$V_{\xi\alpha}(\mathbf{k}) = \sum_{o,\mathbf{n}} e^{i\mathbf{k}\cdot(\mathbf{n}-\mathbf{i})} a_{\alpha o}(\mathbf{k})\langle\varphi_\xi(\mathbf{i})|H|\varphi_o(\mathbf{n})\rangle, \qquad (2)$$

where $\varphi_\xi(\mathbf{i})$ is the impurity $3d$ state at site $\mathbf{i}$, and $\Psi_\alpha(\mathbf{k})$ is the host state with wave vector $\mathbf{k}$ and band index α, which is expanded by atomic orbitals $\varphi_o(\mathbf{n})$ having orbital index o and site index $\mathbf{n}$. Here, N is the total number of host lattice sites, and $a_{\alpha o}(\mathbf{k})$ is an expansion coefficient. To obtain the mixing integrals of $\langle\varphi_\xi(\mathbf{i})|H|\varphi_o(\mathbf{n})\rangle$, we consider a supercell $Ba_8Zn_{15}MnAs_{16}$, which is comprised of 2x2x2 primitive cells, where each primitive cell consists of a $BaZn_2As_2$, and a Zn atom is replaced by an Mn atom. The results of the mixing function $V_{\xi\alpha}(\mathbf{k})$ are shown in Fig. 2 (b) for valence bands, and in Fig. 2 (c) for conduction bands.

The parameters U and ϵ_d are determined as follows. For (Ga,Mn)As, the reasonable parameters are estimated as $U = 4$ eV and $\epsilon_d = $ -2 eV[14]. A recent resonance photoemission spectroscopy experiment showed that the Mn $3d$ partial density of states in $(Ba,K)(Zn,Mn)_2As_2$ and (Ga,Mn)As are quite similar, excepted that the peak of (Ga,Mn)As is approximately 0.4 eV deeper than that of $(Ba,K)(Zn,Mn)_2As_2$[10]. Thus, the reasonable parameters of Mn-doped $BaZn_2As_2$ are $U = 4$ eV and $\epsilon_d = $ -1.5 eV. On the basis of the parameters obtained above, magnetic correlations of the impurities are calculated using the Hirsch−Fye QMC technique with more than 10^6 Monte Carlo sweeps and a Matsubara time step $\Delta\tau = 0.25$.

Figure 3 (a) shows a plot of the occupation number $\langle n_\xi\rangle$ of a ξ orbital of an Mn impurity in $BaZn_2As_2$ against the chemical potential μ at 360 K. The top of the VB was taken to be 0, and the bottom of the CB to be 0.2 eV. Operator n_ξ is defined as follows:

$$n_\xi = n_{\mathbf{i}\xi\uparrow} + n_{\mathbf{i}\xi\downarrow}. \qquad (3)$$

The orbitals xz and yz of Mn subsitutional impurities at the Zn site degenerate owing to the crystal field of $BaZn_2As_2$, which has a group space of I4/mmm[7]. Sharp increases in n_ξ are observed around -0.5, -0.4, -0.2, and 0.0 eV for the orbitals $\xi = z^2$, xy, $x^2 - y^2$, and $xz(yz)$, respectively. This implies the existence of an IBS at this energy ω_{IBS}[13–18]. In order to make the IBS clearer, we show the partial density of state of an Mn impurity, $d\langle n_\xi\rangle/d\mu$, in Fig. 3 (b). The peaks in $d\langle n_\xi\rangle/d\mu$ correspond to the positions of IBS. Figure 3 (c) shows the magnetic correlation $\langle M_{1\xi}^z M_{2\xi}^z\rangle$ between the ξ orbitals of two Mn impurities with fixed distance R_{12} of the first-nearest neighbor. The operator $M_{\mathbf{i}\xi}^z$ of the ξ orbital at impurity site
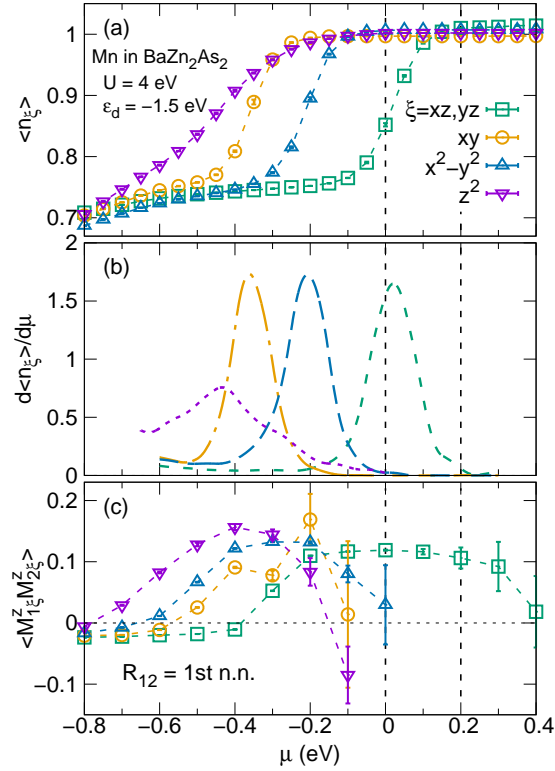
6

FIG. 3. For Mn-doped $BaZn_2As_2$, chemical potential μ dependence of (a) occupation number $\langle n_\xi \rangle$ of ξ orbital of an Mn impurity, (b) partial density of state $d\langle n_\xi \rangle / d\mu$, and (c) magnetic correlation $\langle M_{1\xi}^z M_{2\xi}^z \rangle$ between the ξ orbitals of two Mn impurities with fixed distance R_{12} of the first-nearest neighbor, where the temperature is 360 K. The top of the VB is 0, and the bottom of the CB is 0.2 eV.

i is defined as follows:

$$M_{\mathbf{i}\xi}^z = n_{\mathbf{i}\xi\uparrow} - n_{\mathbf{i}\xi\downarrow}. \tag{4}$$

For each ξ orbital, FM coupling is obtained when the chemical potential μ is close to the IBS position, and FM correlations become weaker and eventually disappear when μ moves away from the IBS. This role of the IBS in determining the strength of FM correlations between impurities is consistent with the Hartree−Fock and QMC results of various DMS systems[13–18].

For Mn-doped $BaZn_2As_2$ with p-type carriers, a recent angle-resolved photoemission spectroscopy (ARPES) experiment showed that the Fermi level (μ) is below the top of the VB by several tenths of an eV and a non-dispersive Mn $3d$ impurity band is present slightly
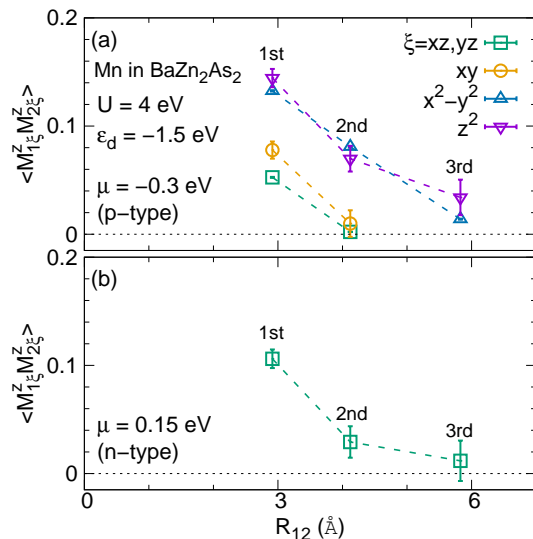
7

FIG. 4. For Mn-doped $BaZn_2As_2$, the distance R_{12} dependence of magnetic correlation $\langle M_{1\xi}^z M_{2\xi}^z \rangle$ between the ξ orbitals of two Mn impurities for the (a) p-type case with chemical potential $\mu = $ -0.3 eV and (b) n-type case with $\mu = 0.15$ eV, where temperature is 360 K. The first-, second-, and third-nearest neighbors of R_{12} are noted.

below the Fermi level[11]. On the basis of the results in Fig. 3 (a), we take $\mu = $ -0.3 eV as an estimate for the p-type case. We argue that the IBS of orbitals xy and z^2, whose positions are below the $\mu = $ -0.3 eV, can account for the non-dispersive Mn $3d$ impurity band below the Fermi level observed in the ARPES experiment. Figure 4 (a) shows the distance R_{12} dependence of the magnetic correlation $\langle M_{1\xi}^z M_{2\xi}^z \rangle$ between the ξ orbitals of two Mn impurities for the p-type case with $\mu = $ -0.3 eV. Long-range FM coupling up to approximately 6 Å(the third nearest neighbor) is obtained for the orbitals $\xi = x^2 - y^2$ and z^2, while short-range FM coupling is obtained for the other three orbitals. Thus, our theoretical results are consistent with the FM observed in the experiment involving Mn-doped $BaZn_2As_2$ with p-type carriers.

For Mn-doped $BaZn_2As_2$ with n-type carriers, a recent experiment showed FM coupling below $T_c = 80$ K[12]. Because no information about the Fermi level has been reported, we take $\mu = 0.15$ eV as an estimate for the n-type case, which is below the bottom of the CB by 0.05 eV. As shown in Fig. 4 (b), long-range FM coupling up to approximately 6 Å(the 3rd nearest neighbor) is obtained for the orbitals $\xi = xz$ and yz. No FM is obtained for the other three orbitals, shown in Fig. 3 (b) as well. A Comparison of Figs. 4(a) and 4(b)
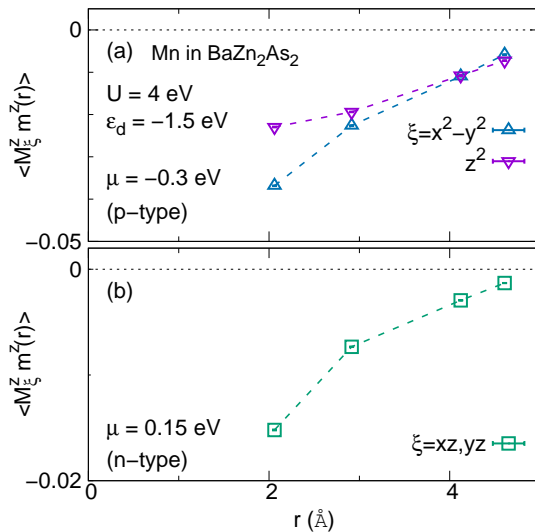
8

FIG. 5. For Mn-doped BaZn$_2$As$_2$, the distance r dependence of magnetic correlation $\langle M_\xi^z m^z(r) \rangle$ between the ξ orbitals of Mn impurity at site origin and the host electron at site $\mathbf{r}$ for the (a) p-type case with chemical potential μ = -0.3 eV and (b) n-type case with μ = 0.15 eV, where temperature is 360 K.

shows that the magnitude of FM coupling $\langle M_{1\xi}^z M_{2\xi}^z \rangle$ in the n-type case is smaller than that in the p-type case, which can qualitatively explain why the T$_c$ in the n-type case[12] is lower than that in the p-type case[7,8] in the experiments.

To understand the long-range FM correlation function $\langle M_1^z M_2^z \rangle$ between two Mn impurities in the BaZn$_2$As$_2$ host, we have calculated the impurity-host magnetic correlation function $\langle M_\xi^z m^z(\mathbf{r}) \rangle$. Here, $\mathbf{r}$ is the site of the host electron and the impurity Mn is located at site $\mathbf{r} = 0$. The magnetization $m^z(\mathbf{r})$ of the host electron at site $\mathbf{r}$ is defined as

$$m^z(\mathbf{r}) = \sum_\alpha (n_{\alpha \mathbf{r} \uparrow} - n_{\alpha \mathbf{r} \downarrow}), \tag{5}$$

where $n_{\alpha \mathbf{r} \sigma} = c_{\alpha \mathbf{r} \sigma}^\dagger c_{\alpha \mathbf{r} \sigma}$ is the number operator for host electrons with band index α and site $\mathbf{r}$ and spin σ. In Fig. 5(a), for p-type carriers with μ = -0.3 eV, the long-range antiferromagnetic (AFM) correlation is obtained between the orbitals $\xi = x^2 - y^2$ and z^2 of Mn impurity and host electrons. In Fig. 5(b), for n-type carriers with μ = 0.15 eV, the long-range AFM correlation is obtained between the orbitals $\xi = xz$ and yz of Mn impurity and host electrons. Thus, the long-range FM coupling between impurities is mediated by the
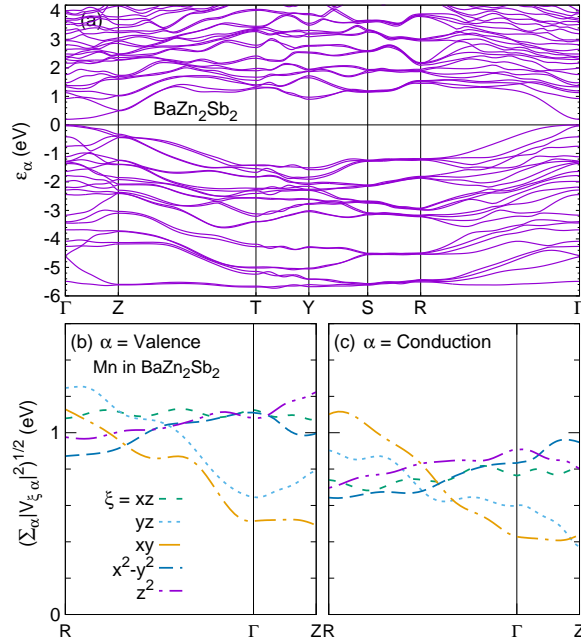
9

FIG. 6. Similar to Fig. 2, with the exception that $BaZn_2As_2$ is replaced by $BaZn_2Sb_2$, which has a different space group Pnma. A direct band gap of 0.2 eV is obtained by DFT calculations, which is in good agreement with the experimental value[29].

polarization of host electron spin. Such carrier-mediated FM is already discussed in previous DMS materials with a wide band gap, such as $(Zn,Mn)O^{13}$, $(Ga,Mn)As^{14}$, and $Mg(O,N)^{15}$.

IV. RESULTS FOR $Ba(Zn, Mn)_2Sb_2$

We made similar calculations for Mn-doped $BaZn_2Sb_2$, where a distinct advantage was the replacement of As with nontoxic Sb. $BaZn_2Sb_2$, too, has a narrow band gap $\Delta_g = 0.2$ eV, but a different space group Pnma[29]. A direct band gap of 0.2 eV was obtained by the DFT calculation as shown in Fig. 6 (a), which agrees well with the experimental value.

Figure 7 (a) shows the occupation number $\langle n_\xi \rangle$ of the ξ orbital of the Mn impurity in $BaZn_2Sb_2$ versus chemical potential μ at temperature 360 K. The $3d$ orbitals of Mn did not degenerate owing to the low symmetry of the crystal field of $BaZn_2Sb_2$. Sharp increases in $\langle n_\xi \rangle$, which imply the position of IBS ω_{IBS}, were observed around -0.6 eV for the xy orbital, -0.4 eV for the yz, x^2-y^2, and z^2 orbitals, and -0.2 eV for the xz orbital. The IBS can be seen more clearly in the partial density of state of an Mn impurity, $d\langle n_\xi \rangle / d\mu$, in Fig. 7 (b). The
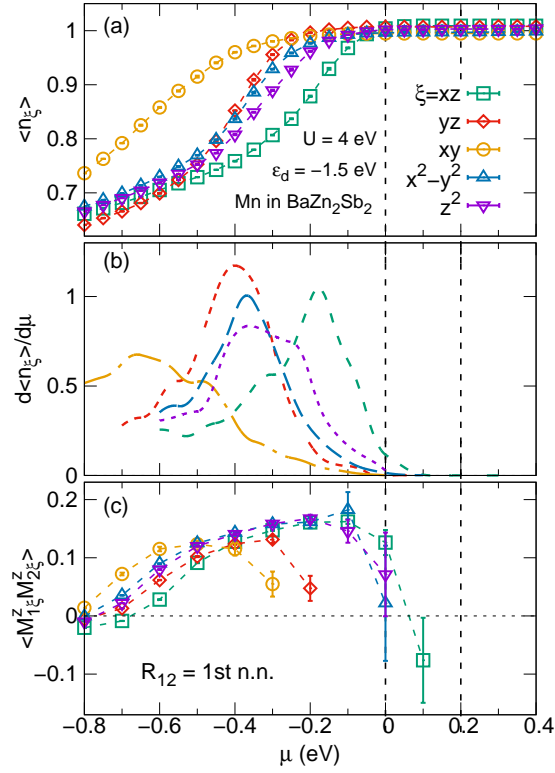
10

FIG. 7. Similar to Fig. 3, except $BaZn_2As_2$ is replaced by $BaZn_2Sb_2$.

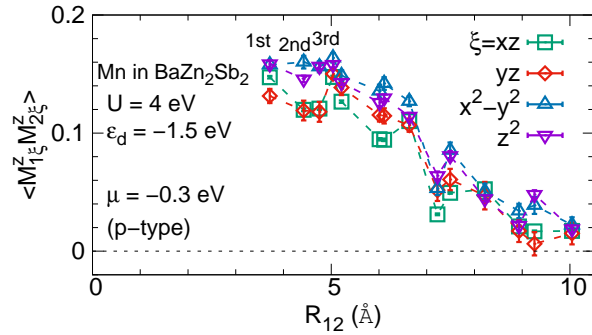

FIG. 8. Similar to Fig. 4(a), except $BaZn_2As_2$ is replaced with $BaZn_2Sb_2$.

peaks in $d\langle n_\xi \rangle / d\mu$ correspond to the positions of the IBS. Figure 7 (c) shows the magnetic correlation $\langle M_{1\xi}^z M_{2\xi}^z \rangle$ between the ξ orbitals of two Mn impurities with fixed distance R_{12} as the first nearest neighbor. The role of the IBS in determining the strength of the FM correlations between impurities is the same as that discussed for Mn-doped $BaZn_2As_2$ in Fig. 3.

For Mn-doped $BaZn_2Sb_2$ with p-type carriers, we take μ = -0.3 eV, the same value as that used for Mn-doped $BaZn_2As_2$ with p-type carriers. Figure 8 shows the distance R_{12} dependence of the magnetic correlation $\langle M_{1\xi}^z M_{2\xi}^z \rangle$ between the ξ orbitals of two Mn impurities for the p-type case. Long-range FM coupling up to approximately 10 Å(the 14th nearest neighbor) was obtained for the $\xi = xz, yz, x^2 - y^2$, and z^2 orbitals, while relatively short-range FM coupling is obtained for the xy orbital. This is considerably longer than 6 Å(the third nearest neighbor) obtained for Mn doped $BaZn_2As_2$ with p-type carriers, as shown in Fig. 4 (a). Such long-range FM coupling arises from the short distance between the neighboring Zn sites in $BaZn_2Sb_2$, as is clear from comparison of the first-, second-, and third-nearest neighbors in Fig. 4(a) and those neighbors in Fig. 8, respectively. We predict that the T_c of Mn-doped $BaZn_2Sb_2$ with p-type carriers should be higher than that of Mn-doped $BaZn_2As_2$ with p-type carriers, in which T_c = 230 K was reported in a recent experiment[8].

For Mn-doped $BaZn_2Sb_2$ with n-type carriers, we take μ = 0.15 eV, the same value as that used for Mn-doped $BaZn_2As_2$ with n-type carriers. No FM coupling is obtained with μ = 0.15 eV. This is because μ = 0.15 eV is far from the IBS position $\omega_{IBS} \approx$ -0.2 eV of the xz orbital, as shown in Figs. 7(a) and 7(b). It is consistent with previous studies that no magnetic coupling is obtained between impurities when $\mu \gg \omega_{IBS}$[13–15].

V. DISCUSSION ON UNCERTAINTY OF MODEL PARAMETERS

In the above QMC calculations, we fix the model parameters of impurity level ϵ_d = -1.5 eV and Coulomb repulsion U = 4 eV, which are reasonable values for Mn-doped $BaZn_2As_2$ and $BaZn_2Sb_2$ as discussed in Sec. III. In this section, we will discuss how the uncertainty of these values affects the outcome of the calculations.

For Mn-doped $BaZn_2As_2$ with the same impurity level parameter ϵ_d = -1.5 eV and a larger Coulomb repulsion parameter U = 5 eV, the occupation number $\langle n_\xi \rangle$, the partial density of state $d\langle n_\xi \rangle/d\mu$ of the ξ orbital of an Mn impurity, and the magnetic correlation $\langle M_{1\xi}^z M_{2\xi}^z \rangle$ between the ξ orbitals of two Mn impurities with fixed distance of the first-nearest neighbor are shown in Figs. 9(a)-9(c), respectively. Compared with the results obtained with parameters ϵ_d = -1.5 eV and U = 4 eV in Fig. 3, no essential difference is observed.

For Mn-doped $BaZn_2As_2$ with a deeper impurity level parameter ϵ_d = -2 eV and the
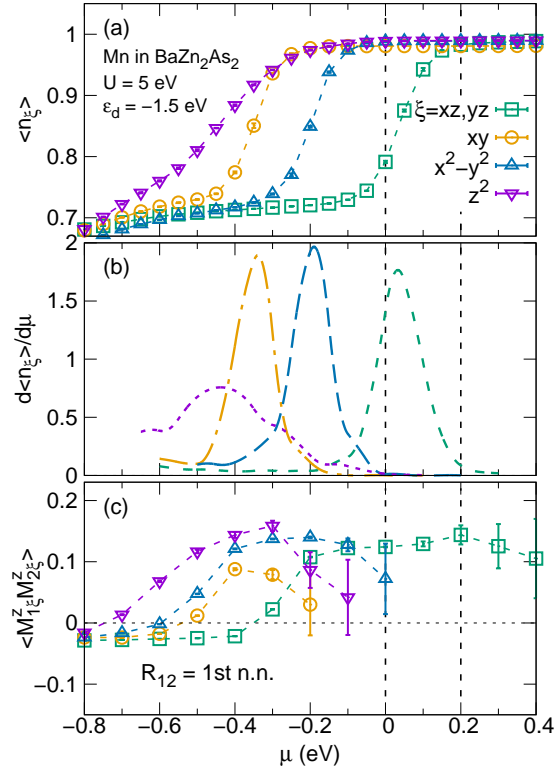
FIG. 9. Similar to Fig. 3, except Coulomb repulsion parameter $U = 4$ eV is replaced by a larger value $U = 5$ eV.

same Coulomb repulsion parameter $U = 4$ eV, $\langle n_\xi \rangle$, $d\langle n_\xi \rangle/d\mu$, and $\langle M_{1\xi}^z M_{2\xi}^z \rangle$ are shown in Figs. 10(a)-10(c), respectively. Compared with the results in Fig. 3, the IBS positions ω_{IBS} of ξ orbitals of Mn impurity shift down by about 0.1 eV. As a result, the FM correlation $\langle M_{1\xi}^z M_{2\xi}^z \rangle$ is obtained for p-type carriers with $\mu = $ -0.3 eV, while no FM correlation $\langle M_{1\xi}^z M_{2\xi}^z \rangle$ is obtained for n-type carriers with $\mu = 0.15$ eV. This result does not agree with the recent experiment of Mn-doped BaZn$_2$As$_2$ with n-type carriers, where FM coupling is observed below T$_c$ = 80 K[12]. Thus, the impurity level parameter $\epsilon_d = $ -2 eV may be too deep for Mn-doped BaZn$_2$As$_2$, as we have also discussed in Sec. III.

For Mn-doped BaZn$_2$Sb$_2$ with the same impurity level parameter $\epsilon_d = $ -1.5 eV and a larger Coulomb repulsion parameter $U = 5$ eV, $\langle n_\xi \rangle$, $d\langle n_\xi \rangle/d\mu$, and $\langle M_{1\xi}^z M_{2\xi}^z \rangle$ are shown in Figs. 11(a)-11(c), respectively. Compared with the results obtained with parameters $\epsilon_d = $ -1.5 eV and $U = 4$ eV in Fig. 7, no essential difference is observed.

For Mn-doped BaZn$_2$Sb$_2$ with a deeper impurity level parameter $\epsilon_d = $ -2.0 eV and the
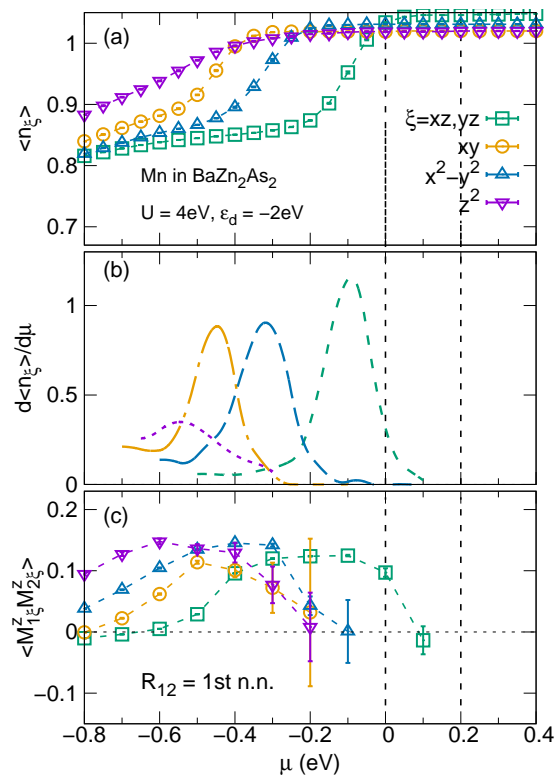
FIG. 10. Similar to Fig. 3, except impurity level parameter ϵ_d = -1.5 eV is replaced by a deeper value ϵ_d = -2 eV.

same Coulomb repulsion parameter $U = 4$ eV, $\langle n_\xi \rangle$, $d\langle n_\xi \rangle / d\mu$, and $\langle M_{1\xi}^z M_{2\xi}^z \rangle$ are shown in Figs. 12(a)-12(c), respectively. Compared with the results in Fig. 7, the IBS positions ω_{IBS} of ξ orbitals of Mn impurity shift down by about 0.1 eV. The FM correlation $\langle M_{1\xi}^z M_{2\xi}^z \rangle$ is obtained for p-type carriers with μ = -0.3 eV, and no FM correlation $\langle M_{1\xi}^z M_{2\xi}^z \rangle$ is obtained for n-type carriers with μ = 0.15 eV. The conclusion is unchanged.

VI. CONCLUSIONS

In summary, we have proposed a method to realize DMS with p- and n-type carriers by choosing host semiconductors with a narrow band gap. Using the combined method of DFT and QMC, we describe DMS Mn-doped $BaZn_2As_2$, which has a narrow band gap of 0.2 eV. In addition, we find a nontoxic DMS Mn-doped $BaZn_2Sb_2$, whose T_c is expected to be higher than that of Mn-doped $BaZn_2As_2$, for which $T_c = 230$ K, as reported in a recent
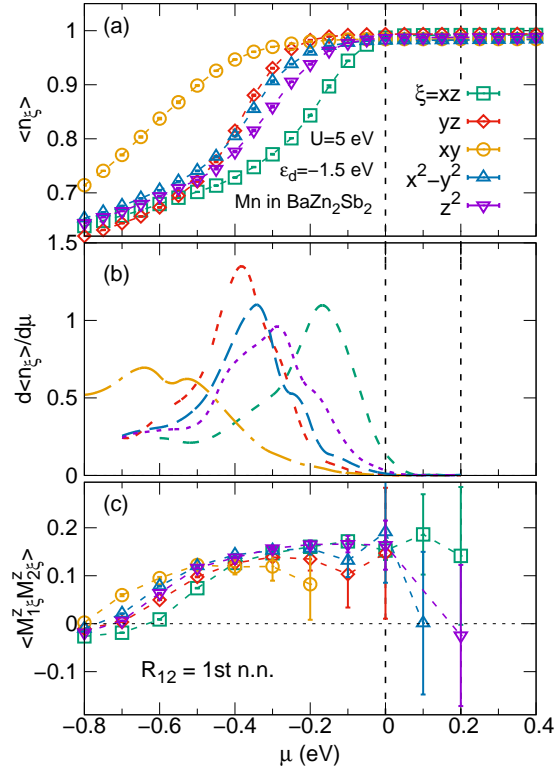
FIG. 11. Similar to Fig. 7, except Coulomb repulsion parameter $U = 4$ eV is replaced by a larger value $U = 5$ eV.

experiment.

* Corresponding author: gu.bo@jaea.go.jp

[1] H. Ohno, Science **281**, 951 (1998).

[2] T. Dietl, Nat. Mater. **9**, 965 (2010).

[3] M. Wang, R. P. Campion, A. W. Rushforth, K. W. Edmonds, C. T. Foxon, and B. L. Gallagher, Appl. Phys. Lett. **93**, 132103 (2008).
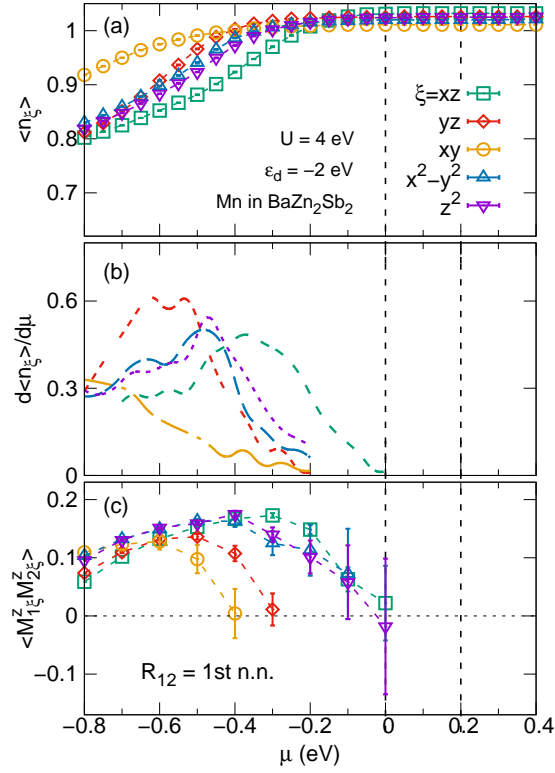
FIG. 12. Similar to Fig. 7, except impurity level parameter ϵ_d = -1.5 eV is replaced by a deeper value ϵ_d = -2 eV.

[4] J. Masek, J. Kudrnovsky, F. Maca, B. L. Gallagher, R. P. Campion, D. H. Gregory, and T. Jungwirth, Phys. Rev. Lett. **98**, 067202 (2007).

[5] Z. Deng, C. Q. Jin, Q. Q. Liu, X. C. Wang, J. L. Zhu, S. M. Feng, L. C. Chen, R. C. Yu, C. Arguello, T. Goko, F. Ning, J. Zhang, Y. Wang, A. A. Aczel, T. Munsie, T. J. Williams, G. M. Luke, T. Kakeshita, S. Uchida, W. Higemoto, T. U. Ito, B. Gu, S. Maekawa, G. D. Morris, and Y. J. Uemura, Nat. Commun. **2**, 422 (2011).

[6] Z. Deng, K. Zhao, B. Gu, W. Han, J. L. Zhu, X. C. Wang, X. Li, Q. Q. Liu, R. C. Yu, T. Goko, B. Frandsen, L. Liu, J. Zhang, Y. Wang, F. L. Ning, S. Maekawa, Y. J. Uemura, and C. Q. Jin, Phys. Rev. B **88**, 081203(R) (2013).

[7] K. Zhao, Z. Deng, X. C. Wang, W. Han, J. L. Zhu, X. Li, Q. Q. Liu, R. C. Yu, T. Goko, B. Frandsen, L. Liu, F. L. Ning, Y. J. Uemura, H. Dabkowska, G. M. Luke, H. Luetkens, E. Morenzoni, S. R. Dunsiger, A. Senyshyn, P. Boni, and C. Q. Jin, Nat. Commun. **4**, 1442 (2013).

[8] K. Zhao, B. J. Chen, G. Q. Zhao, Z. Yuan, Q. Q. Liu, Z. Deng, J. L. Zhu, and C. Q. Jin, Chin. Sci. Bull. **59**, 2524 (2014).

[9] J. K. Glasbrenner, I. Zutic, and I. I. Mazin, Phys. Rev. B **90**, 140403(R) (2014).

[10] H. Suzuki, K. Zhao, G. Shibata, Y. Takahashi, S. Sakamoto, K. Yoshimatsu, B. J. Chen, H. Kumigashira, F. H. Chang, H. J. Lin, D. J. Huang, C. T. Chen, B. Gu, S. Maekawa, Y. J. Uemura, C. Q. Jin, and A. Fujimori, Phys. Rev. B **91**, 140401(R) (2015).

[11] H. Suzuki, G. Q. Zhao, K. Zhao, B. J. Chen, M. Horio, K. Koshiishi, J. Xu, M. Kobayashi, M. Minohara, E. Sakai, K. Horiba, H. Kumigashira, B. Gu, S. Maekawa, Y. J. Uemura, C. Q. Jin, and A. Fujimori, Phys. Rev. B **92**, 235120 (2015).

[12] H. Y. Man, C. Ding, S. L. Guo, G. X. Zhi, X. Gong, Q. Wang, H. D. Wang, B. Chen, and F. L. Ning, arXiv:1403.4019 (unpublished).

[13] B. Gu, N. Bulut, and S. Maekawa, J. Appl. Phys. **104**, 103906 (2008).

[14] J. Ohe, Y. Tomoda, N. Bulut, R. Arita, K. Nakamura, and S. Maekawa, J. Phys. Soc. Jpn. **78**, 083703 (2009).

[15] B. Gu, N. Bulut, T. Ziman, and S. Maekawa, Phys. Rev. B **79**, 024407 (2009).

[16] M. Ichimura, K. Tanikawa, S. Takahashi, G. Baskaran, and S. Maekawa, *Foundations of Quantum Mechanics in the Light of New Technology*, edited by S. Ishioka and K. Fujikawa. (World Scientific, Singapore, 2006), pp. 183-186.

[17] N. Bulut, K. Tanikawa, S. Takahashi, and S. Maekawa, Phys. Rev. B **76**, 045220 (2007).

[18] Y. Tomoda, N. Bulut, and S. Maekawa, Physica B **404**, 1159 (2009).

[19] P. Hohenberg and W. Kohn, Phys. Rev. **136**, B864 (1964).

[20] W. Kohn and L. J. Sham, Phys. Rev. **140**, A1133 (1965).

[21] J. E. Hirsch and R. M. Fye, Phys. Rev. Lett. **56**, 2521 (1986).

[22] B. Gu, J. Y. Gan, N. Bulut, T. Ziman, G. Y. Guo, N. Nagaosa, and S. Maekawa, Phys. Rev. Lett. **105**, 086401 (2010).

[23] B. Gu, I. Sugai, T. Ziman, G. Y. Guo, N. Nagaosa, T. Seki, K. Takanashi, and S. Maekawa, Phys. Rev. Lett. **105**, 216401 (2010).

[24] Z. Xu, B. Gu, M. Mori, T. Ziman, and S. Maekawa, Phys. Rev. Lett. **114**, 017202 (2015).

[25] F. D. M. Haldane and P. W. Anderson, Phys. Rev. B **13**, 2553 (1976).

[26] P. Blaha, K. Schwart, G. K. H. Hadsen, D. Kvasnicka, and J. Luitz, WIEN2K, An Augmented Plane Wave Plus Local Orbitals Program for Calculating Crystal Properties, Vienna University

of Technology, Vienna, 2001.

[27] F. Tran and P. Blaha, Phys. Rev. B **83**, 235118 (2011).

[28] I. R. Shein and A. L. Ivanovskii, J. Alloys Compd. **583**, 100 (2014).

[29] G. K. H. Madsen, J. Am. Chem. Soc. **128**, 12140 (2006).